Dry and warm conditions in Australia exacerbated by aerosol reduction in China

Jiyuan Gao[1], Yang Yang[1*], Hailong Wang[2], Pinya Wang[1], Hong Liao[1]

[1]Joint International Research Laboratory of Climate and Environment Change (ILCEC), Jiangsu Key Laboratory of Atmospheric Environment Monitoring and Pollution Control, Jiangsu Collaborative Innovation Center of Atmospheric Environment and Equipment Technology, School of Environmental Science and Engineering, Nanjing University of Information Science and Technology, Nanjing, Jiangsu, China

[2]Atmospheric, Climate, and Earth Sciences Division, Pacific Northwest National Laboratory, Richland, Washington, USA

*Correspondence to yang.yang@nuist.edu.cn

Abstract

A substantial decline in anthropogenic aerosols in China has been observed since the initiation of clean air actions in 2013. Concurrently, Australia experienced anomalously dry and warm conditions ~~in~~since the 2010s. This study reveals a linkage between aerosol reductions in China and the drying and warming trends in Australia during 2013–2019 based on ~~aerosol~~ fully-coupled climate model simulations and multi-source observations. Aerosol decline in China triggered alterations in temperature and pressure gradients between the two hemispheres, leading to intensified outflow from Asia towards the South Indian Ocean, strengthening the Southern Indian Subtropical High and its related Southern Trade Winds. Consequently, this atmospheric pattern resulted in a moisture divergence over Australia. The reduction in surface moisture further resulted in more surface energy being converted into sensible heat instead of evaporating as latent heat, warming the near-surface air. Aerosol reductions in China are found to contribute to ~~19% of~~ the ~~observed~~ decreases in precipitation and relative humidity and ~~8% of~~ the increase in surface air temperature in Australia during 2013–2019. The intensified dry and warm climate conditions during 2013–2019 further ~~explain 12%–19% of~~caused the increase in wildfire risks during fire seasons in Australia. Our study illuminates the impact of distant aerosols on precipitation and temperature variations in Australia, offering valuable insights for drought and wildfire risk mitigation in Australia.

1 Introduction

47

48   Australia encompasses various climate zones, ranging from the tropical climate in the north

49 to arid conditions in the interior and temperate climates in the south (Head et al., 2014). The

50 continent is predominantly dry, receiving an average annual rainfall of less than 600 mm and less

51 than 300 mm over half of the land. Evident long-term trends can be observed in Australia's

52 historical rainfall records. These trends reveal a notable shift towards drier conditions across

53 southern Australia (Dey et al., 2019a; Nicholls, 2006; Rauniyar and Power, 2020; Wasko et al.,

54 2021), and an increase in rainfall before 2010 (Dey et al., 2019a, b; Evans et al., 2014; Nicholls,

55 2006; Rotstayn et al., 2007; Wasko et al., 2021) followed by a slight decreasing trend of rainfall

56 after 2010 (CSIRO and BOM, 2022) in the northern Australia.

57   Precipitation in Australia is influenced by a variety of atmospheric circulation systems,

58 including East Coast Lows (ECLs), the Australian-Indonesian Monsoon, tropical cyclones (TCs),

59 fronts, and different modes of large-scale climate variabilities, such as the El Niño-Southern

60 Oscillation (ENSO), Indian Ocean Dipole (IOD), Interdecadal Pacific Oscillation (IPO),

61 Subtropical ridge (STR), Southern Annular Mode (SAM), and Madden Julian Oscillation (MJO)

62 (Dey et al., 2019a; Risbey et al., 2009). The linkages between Australia's rainfall characteristics

63 and these drivers could change in response to the internal natural variabilities and external

64 anthropogenic forcings. Rauniyar and Power (2020) reported that the drier conditions across the

65 southern Australia could be attributed to a combination of both decadal-scale natural variability

66 and changes in large-scale atmospheric circulation patterns, which was linked to the escalating

67 emissions of greenhouse gases (GHGs), while Rotstayn et al. (2007) found that the increased levels

68 of rainfall in northern Australia before 2010 was linked to the increases in aerosols in Asia.

69   Human activities have led to a rise of global surface air temperature by approximately 1.29 °C

70 (0.99 to 1.65 °C) from 1750 to 2019, mainly due to an enhanced greenhouse effect from increasing

71 ~~GHGs~~GHG emissions (IPCC, 2021). In addition to GHGs, human activities also emit a variety of

72 aerosols and their gaseous precursors into the atmosphere. Since industrialization, there has been

73 a significant rise in the levels of aerosols and precursors (Hoesly et al., 2018). ~~These~~

74 ~~atmospheric~~Atmospheric aerosols ~~play a crucial role in changing the earth's radiation balance,~~

75 ~~both directly and indirectly, and are considered as~~are the second-largest anthropogenic climate

76 forcer following GHGs, exerting an overall cooling effect that partially masks the warming

77 induced by GHGs. (IPCC, 2013, 2021). However, as anthropogenic aerosols declined during the

78 past decades in many countries of the world related to the clean air actions, the associated "unmask"

79 effect is likely to exacerbate GHG-induced warming (Kloster et al., 2010). For example, in the

80 1980s, clean air actions were implemented in North America and Europe, leading to a decrease in

81 the emissions of aerosols and their precursors (Hoesly et al., 2018). Reductions in aerosol

82 emissions in the U.S. have led to changes in aerosol direct radiative forcing (DRF) by 0.8 W m^{-2}

83 and indirect radiative forcing (IRF) by 1.0 W m^{-2} over the eastern U.S. during 1980–2010

84 (Leibensperger et al., 2012). Similarly, aerosol decreases over Europe between the 1980s and

85 1990s have caused a change in regional DRF by 1.26 W m^{-2} (Pozzoli et al., 2011). In China, the

86 emissions of aerosols and their precursors have been reduced since 2013 due to the implementation

87 of Air Pollution Prevention and Control Action Plan. Dang and Liao (2019) reported a 1.18 W m^{-2}

88 change in DRF between 2012 and 2017 due to decreased aerosol levels over eastern China. Gao

89 et al. (2022) estimated a warming of 0.20 °C in China, 0.15 °C in North America, and 0.14 °C in

90 Europe, attributed to the decreases in aerosols during 2013–2019.

91 Monsoonal rainfall serves as a vital resource for agriculture, industry, and ecosystems across

92 the monsoon-affected regions, affecting approximately two-thirds of the world's population (B.

93 Wang et al., 2021). Apart from GHGs-induced warming (Cook and Seager, 2013) and nature

94 variabilities (e.g., ENSO) (Oh and Ha, 2015), aerosol also modulates monsoon system mainly

95 through changing land-sea temperature and pressure gradient. The impact of aerosols on Asian

96 monsoon has been widely investigated. Based on climate model simulations, Liu et al. (2023)

97 found that aerosol reductions in East Asia during 2013–2017 resulted in an approximately 5%

98 increase in the strength of the East Asian summer monsoon (EASM). The EASM is also reported

99 to enhance due to future aerosol reductions from 2000 to 2100 (Wang et al., 2016). Dong et al.

100 (2019) explored the effects of increased aerosol in Asia from 1970s to 2000s on atmospheric

101 circulation and rainfall patterns and found anomalous moisture convergence and increased

102 precipitation over the Maritime continent. Non-Asian aerosols also have an effect on South Asian

103 monsoon rainfall through changes in the interhemispheric temperature gradient and meridional

104 shifts of the Intertropical Convergence Zone (Bollasina et al., 2011, 2014; Cowan and Cai, 2011;

105 Undorf et al., 2018). Australia, especially thein northern Australia, is largely affected by the

106 Australian monsoon, which is characterized by winds that blow from the southeast during cold

season and from the northwest during the warm season (Gallego et al., 2017; Heidemann et al., 2023). Australia has a relatively low level of anthropogenic aerosols, which suggests that the impact of domestic anthropogenic aerosols on Australian monsoon should not be significant. However, the impact of remote aerosols on Australian monsoon have been investigated in previous studies, and they reported that the increases in Asian aerosols could enhance rainfall in Australia through increasing monsoonal winds towards Australia (Rotstayn et al., 2007; Fahrenbach et al., 2023).

Wildfires, which are uncontrolled fires spreading rapidly across natural landscapes, are significantly influenced by meteorological conditions (He et al., 2019; Jones et al., 2022). In Australia, these fires, also known as bushfires, present a major environmental and social threat (Johnston et al., 2021; Ward et al., 2020). According to Dowdy (2020), the most favorable seasons for wildfires in most regions of Australia are austral spring and summer. Key meteorological factors such as extended periods of drought, elevated temperatures, low humidity, and strong winds are crucial in determining the occurrence and intensity of wildfires (Zacharakis and Tsihrintzis, 2023). Under the recent historical climate change, Australia has witnessed a rise in extreme fire weather conditions and an extended fire season (CSIRO and BOM, 2022).

Since the implementation of clean air policies in 2013, there has been a noticeable decrease in aerosol levels in China (Zhang et al., 2019; Zheng et al., 2018). Numerous studies have shown the local and global climate effects of the aerosol reductions in China (Dang and Liao, 2019; Gao et al., 2022, 2023; Liu et al., 2023; Zheng et al., 2020). The Australian monsoonal wind patterns, reported to be influenced by Asian aerosol emissions in the past decades (Rotstayn et al., 2007; Fahrenbach et al., 2023), may have also influenced by the radiative effects due to the aerosol decline in China. The objective of this study is to assess the worsened dry and warm conditions and associated wildfire risk in Australia during 2013–2019 and investigate the possible linkage between the changes in climate conditions in Australia and anthropogenic aerosols.

2 Methods

2.1 Observational and Reanalysis Data

Ground-based observational data of near-surface $PM_{2.5}$ concentrations in China 2013–2019

135 are acquired from the China National Environmental Monitoring Centre (CNEMC), which offers

136 daily records of near-surface air pollutant concentrations for nearly 1800 sites. Aerosol Optical

137 Depth (AOD) data are obtained from the Moderate Resolution Imaging Spectroradiometer

138 (MODIS) Deep Blue retrieval (Hsu et al., 2013). These observational data are used for evaluating

139 the performance of model simulated aerosols.

140 ERA5, the fifth generation of the European Centre for Medium-range Weather Forecasts

141 (ECMWF) atmospheric reanalysis, is a comprehensive dataset that provides a detailed and globally

142 consistent view of the earth's atmospheric conditions over the past several decades (Hersbach et

143 al., 2020). In this study, ERA5 data are employed to evaluate the climate condition in Australia

144 and analyze its linkage with aerosol reductions in China during the 2013–2019 by using the 2-

145 meter temperature, total precipitation, relative humidity, cloud cover, wind fields, vertical velocity,

146 surface latent and sensible heat flux, and surface and top of the atmosphere (TOA) solar and

147 longwave radiative flux under both clear and all sky conditions.

148 ~~Clouds and the Earth's Radiant Energy System-Energy Balanced and Filled (CERES-EBAF)~~

149 ~~is a dataset that provides information on the earth's radiation budget, including surface and TOA~~

150 ~~energy fluxes (Loeb et al., 2018). It combines data from satellite instruments to estimate how much~~

151 ~~energy the earth receives from the sun and how much is reflected back to space, helping to~~

152 ~~understand climate change and energy balance processes. The variables used in the study include~~

153 ~~cloud cover and surface and TOA solar and longwave radiative fluxes under both clear and all sky~~

154 ~~conditions.~~

155 The Global Precipitation Measurement (GPM) mission is a joint initiative by National

156 Aeronautics and Space Administration (NASA) and the Japan Aerospace Exploration Agency

157 (JAXA) aimed at providing accurate and frequent measurements of global precipitation

158 (Skofronick-Jackson et al., 2017). GPM includes a core satellite equipped with advanced radar and

159 microwave sensors, enabling the observation of rain and snowfall in real-time. The data are crucial

160 for understanding weather patterns, climate dynamics, and hydrological processes. The Global

161 Precipitation Climatology Project (GPCP) is an international initiative under the World Climate

162 Research Programme (WCRP) that integrates satellite and gauge-based observations to provide

163 long-term, global precipitation estimates (Adler et al., 2018). ~~Precipitation rate data from GPM are~~

164 ~~also used in the study~~GPCP offers monthly and daily precipitation datasets with global coverage,

165 combining data from rain gauges, satellite infrared (IR), and microwave sensors to enhance

166 accuracy. Precipitation rate data from GPM and GPCP are also used in the study. GPM provides

167 higher temporal and spatial resolution data compared to Global Precipitation Climatology Project

168 (GPCP), making it more suitable for studies focused on short-term precipitation variability and

169 regional climate dynamics.

2.2 Model Description and Experimental Design

171   In this research, we conduct simulations to explore the impact of aerosols on climate using

172 the Community Earth System Model version 1 (CESM1). CESM1 simulates the major aerosols

173 including sulfate, black carbon (BC), primary organic matter (POM), secondary organic aerosol

174 (SOA), dust and sea salt in a four-mode Modal Aerosol Module (MAM4), as described in Liu et

175 al. (2016). CESM1 simulations are carried out with 30 vertical layers and a horizontal resolution

176 of 2.5° longitude by 1.9° latitude. In addition to the default model physics, several supplementary

177 features are incorporated into the model in this study to improve the model's performance in

178 simulating aerosol wet scavenging and convective transport (Wang et al., 2013).

179   The global anthropogenic emissions of aerosols and their precursors are obtained from the

180 Community Emissions Data System (CEDS) v_2021_04_21. In contrast to the prior CEDS

181 v_2016_07_26, which exhibits significant regional emission biases (Z. Wang et al., 2021), the

182 newer CEDS version of anthropogenic emissions of aerosols and precursors considers the

183 substantial reductions in emissions in China, related to the recent clean air actions since 2013 (Fig.

184 S1). Specifically, anthropogenic sulfur dioxide (SO_2), BC, and organic carbon (OC) emissions

185 decreased by −12.48, −0.30, and −0.21 Tg yr^{-1}, respectively, over China between 2013 and 2019.

186 Biogenic emissions are from the Model of Emissions of Gases and Aerosols from Nature version

187 2.1 (MEGAN v2.1) (Guenther et al., 2012), while the emissions from open biomass burning are

188 derived from the CMIP6 (Coupled Model Intercomparison Project Phase 6) (Van Marle et al.,

189 2017).

190   A series of model experiments are conducted using CESM1 with a fully-coupled model

191 configuration, as detailed in Table S1. In the baseline scenario (referred to as BASE),

192 anthropogenic emissions of aerosols and precursors are fixed at year 2013 worldwide. In CHN,

193   anthropogenic emissions of aerosols and precursors over China are fixed at year 2019, while

194   emissions in all other regions are remained at year 2013. In NAEU, the simulation is performed

195   with anthropogenic emissions of aerosols and precursors over North America and Europe set at

196   year 2019, while emissions in other regions remained at year 2013. In OTH, anthropogenic

197   emissions of aerosols and precursors in other regions except for China are set at year 2019, while

198   emissions in China are kept at year 2013. Biogenic and biomass burning emissions worldwide in

199   all experiments are fixed at year 2013. To reduce model biases related to internal variability, three

200   ensemble members are conducted by perturbing the initial atmospheric temperature conditions.

201   All simulations are run for 150 years, with the last 100 years for detailed analysis.

202   **2.3 Model Evaluation**

203   To validate whether CESM1 can reproduce the aerosol reductions in China during the 2010s,

204   changes in simulated near-surface $PM_{2.5}$ concentrations (sum of sulfate, BC, POM, SOA, dust×0.1,

205   and sea-salt×0.25 following Turnock et al. (2020)) in China during 2013–2019 are compared with

206   the observations. Figure S2 shows spatial distributions of observed and modeled annual mean near-

207   surface $PM_{2.5}$ concentration changes over China (2017–2019 minus 2013–2015), which exhibited

208   a statistically significant correlation coefficient of 0.52 between simulations and observations.

209   However, the model underestimates the $PM_{2.5}$ concentration changes by 76% in China. The

210   considerable underestimation has been reported in many previous studies, resulting from coarse

211   model resolution, uncertainties in emissions of aerosols and precursor gases, strong aerosol wet

212   removal, and the model's deficiency in simulating nitrate and ammonium aerosols (Fan et al., 2018,

213   2022; Gao et al., 2022, 2023; Zeng et al., 2021). The model has a good capability in replicating

214   the spatial distribution of AOD changes in China during 2013–2019 (Fig. S3), as evidenced by a

215   high correlation coefficient of 0.83, but the model also exhibits an underestimation in the AOD

216   reductions by 69%. However, the apparent underestimation of absolute changes may largely stem

217   from the inherently low background aerosol concentrations in CESM1. When considering the

218   relative changes rather than absolute values, the bias appears much less pronounced (Fig. S4 and

219   Fig. S5).

220   Climate variables, including precipitation rate, surface air temperature, relative humidity,

221   total cloud cover, surface solar radiation, 10m wind speed, and surface and TOA net total radiative

222 fluxes under both clear and all sky conditions over Australia simulated by CESM1 model are also

223 compared with those from ERA5 reanalysis (Fig. ~~S4~~ S6 S8). The model demonstrates a good

224 performance in simulating Australian climate, with normalized mean bias (NMB) values

225 consistently below or near 40% for surface air temperature, relative humidity, total cloud cover,

226 surface downward solar radiation, and 10m wind speed, and surface and TOA net total radiative

227 fluxes, but it tends to overestimate annual precipitation by about 90%, especially over coastal

228 regions likely related to the coarse model resolution. The model accurately reproduces spatial

229 patterns of all climate variables, closely aligning with observations, as indicated by correlation

230 coefficients ranging from 0.7 to 1.0.

231 **2.4 Wildfire Risk Indices**

232 In this study, several climatological indices are used to indicate wildfire risk during fire

233 seasons (austral spring and summer, from September to February of the next year) in Australia

234 (Ren et al., 2022; Irmak et al., 2003; Seager et al., 2015; Sharples et al., 2009).

235 (i) Reference Potential Evapotranspiration (ET_0):

236 ET_0 is a climatological index used to estimate the amount of water that could potentially

237 evaporate and be transpired from the ~~earth's~~ Earth's surface under specific meteorological

238 conditions. The calculation of ET_0 takes into account factors such as temperature (T, unit: °C), and

239 surface downward solar radiation (R_s, unit: W m^{-2}) to estimate the maximum amount of water loss

240 due to evaporation and transpiration. ET_0 is important in wildfire studies because it helps to gauge

241 the environmental moisture conditions and the potential for drought, which can be a significant

242 factor in wildfire risks assessment. ET_0 is given by the following expression (Irmak et al., 2003):

$$ET_0 = -0.611 + 0.149R_s + 0.079\text{T}$$

244 (ii) Vapor Pressure Deficit (VPD):

245 Vapor Pressure Deficit (VPD) is a meteorological parameter that measures the difference

246 between the amount of moisture in the air and the maximum amount of moisture the air can hold

247 at a given temperature (T, unit: °C) and moisture (relative humidity, RH, unit: %). High VPD

248 values indicate that the air is dry. VPD is important in the context of wildfires because it reflects

249   the drying potential of the atmosphere. When VPD is high, it can lead to rapid moisture loss from

250   vegetation, making it more susceptible to ignition and increasing the risk of wildfires. VPD is

251   given by (Seager et al., 2015):

252
$$VPD = \frac{100 - RH}{100} \times 610.7 \times 10^{\frac{7.5T}{237.3+T}}$$

253   (iii) McArthur Forest Fire Danger Index (FFDI):

254   The McArthur Forest Fire Danger Index (FFDI) is a widely used index in Australia to assess

255   the potential for bushfires and forest fires. It takes into account various meteorological factors,

256   including T (unit: °C), RH (unit: %), wind speed (U, unit: m s^{-1}), and drought factor (DF, unitless).

257   We set DF as 10 here following Sharples et al. ~~(2009).~~(2009), as it would not significantly affect

258   the methods of comparison used later in their study. While we acknowledge that this assumption

259   is idealized, we find it applicable in our case. To verify this, we calculated gridded DFs for

260   Australia (Figure S9), which show that the DFs are close to 10 and exhibit nearly homogeneous

261   spatial distributions. As such, setting DF = 10 for Australia is reasonable for our analysis. In

262   addition, FFDI calculated using DF = 10 and FFDI using gridded DFs are compared (Figure S10).

263   The patterns and regional averages of both datasets are very similar, further supporting the use of

264   DF = 10 in our study. The FFDI provides a numerical rating that indicates the level of fire danger,

265   with higher values corresponding to greater fire risks. This index is particularly valuable for

266   assessing the immediate risk of wildfires and is commonly used in fire management and prediction.

267   FFDI is defined as (Sharples et al., 2009):

268
$$FFDI = 2e^{-0.45+0.987lnDF+0.0338T-0.0345RH+0.0234U}$$

269   **3 Results**

270   **3.1 Intensified Dry and Warm Conditions in Australia by aerosol changes**

271   Figure 1 shows simulated responses in annual ~~and seasonal~~ precipitation rate, surface air

272   temperature and relative humidity in Australia to changes in anthropogenic emissions of aerosols

273   and precursors ~~in China~~. In response to aerosol reductions in China, Australia experiences

274   significant decreases in precipitation and relative humidity, while the temperature has an increase

275   from 2013 to 2019. On regional average, annual precipitation, surface air temperature and relative

276   humidity change by -0.10 mm day^{-1}, 0.06 °C, and -1.20%, respectively, in Australia caused by

277   the aerosol reduction in China during this time period, contributing to the dry and warm climate in

278   Australia. Notably, Northern Australia experiences the most significant reduction in convective

279   precipitation, whereas Southern Australia has the greatest decline in large-scale precipitation

280   related to the aerosol reduction in China, as simulated by the CESM1 model (Fig. ~~S7~~S11). The

281   direction of seasonal responses in precipitation rate, surface air temperature and relative humidity

282   are the same as the annual averages, with the largest changes occurring in austral spring (Fig. ~~1~~2).

283   The intensified dry and warm conditions in Australia can also be seen in the observations,

284   as indicated by ERA5 reanalysis data (Fig. ~~2).~~3). Since 2010, precipitation and relative humidity

285   have significantly decreased in Australia, especially in Northern and Eastern Australia, at a rate of

286   0.086 mm day^{-1} yr^{-1} and 1.07% yr^{-1}, respectively, while surface air temperature has increased at a

287   rate of 0.17 °C yr^{-1}. ~~The decrease in precipitation in Australia is also reflected in the GPM data~~

288   ~~(Fig. S8). It translates into the changes in precipitation, temperature and relative humidity by 0.52~~

289   ~~mm day^{-1}, 1.0 °C and 6.4% in Australia during 2013–2019 in observations if the trends are~~

290   ~~assumed to be linear. This suggests that aerosol reductions in China can explain 19% of the~~

291   ~~decreases in precipitation and relative humidity and 8% of the increase in surface air temperature~~

292   ~~in Australia during 2013–2019, worsening the dry and warm climate conditions in Australia (Fig.~~

293   ~~S9).~~In addition, Time series of precipitation have also been extended to cover 2001–2019, clearly

294   showing an increasing precipitation trend during 2001–2010, followed by a decreasing trend

295   during 2010–2019 (Fig. S12). It is in accordance with the increasing aerosols in China before 2010

296   and aerosol reduction in recent years. To account for the potential influence of internal variability,

297   particularly ENSO, which is a major driver of Australia's precipitation variability (Fig. S13), the

298   time series are also given after removing the influence of Niño 3.4 index. The adjusted results

299   exhibit a similar transition, confirming the robustness of the observed drying trend since the 2010s

300   (Fig. S12). The GPM and GPCP data also exhibit a similar decreasing trend in precipitation over

301   Australia (Fig. S14). The reduction in anthropogenic SO_2 emissions in China shows strong

302   correlations with the decrease in precipitation and the increase in temperature in Australia during

303   2010–2019 (Fig. ~~S10~~S15). However, when extending the time frame to the period before emissions

304   reductions in China (1940–2019), the increase in temperature becomes less pronounced, with a

305   slight rise in precipitation and relative humidity, likely attributed to greenhouse gas warming,

306 which can serve as ~~evidence~~indication that the decrease in precipitation and increase in

307 temperature in Australia from 2010 to 2019 are not primarily caused by GHGs (~~Figure S11~~Fig.

308 S16). The rainfall decrease is consistent with changes in clouds. Spatial distributions of simulated

309 changes in vertically-integrated cloud cover ~~and the linear trends in observations are shown in Fig.~~

310 ~~S12–S14. In both observation and model simulation, the results consistently indicate~~are shown in

311 Figure S17, indicating a reduction in clouds of all levels, including high, mid-level, and low clouds.

312 In addition, the spatial distributions of these changes closely resemble the patterns of responses in

313 precipitation and relative humidity.

314 Aerosol emissions have changed across the world rather than in China alone during 2013–

315 2019, such as those in Australia, North America and Europe, which affect climate in both local

316 and remote regions. ~~Figures S15a and S15b~~Figure 1 also shows changes in ~~precipitation and~~

317 ~~surface temperature~~climate variables in Australia due to changes in other regions except China.

318 The aerosol changes in other regions except China yield a decrease in precipitation by 0.06 mm

319 day^{-1} ~~and,~~ an increase in temperature by 0.06 °C~~, which are similar to those caused~~ and a decrease

320 in relative humidity by ~~the aerosol changes in China (Fig. 1).~~0.67%. In particular, North America

321 and Europe emission changes ~~largely~~, to some extent, contribute to the responses in precipitation

322 (–0.04 mm day^{-1}~~) and~~), temperature (0.04 °C) and relative humidity (–0.41%) attributed to other

323 regions (except China), although the responses are mostly insignificant (~~Figs. 15c and 15d~~Fig. 1).

324 **3.2 Mechanisms of Dry and Warm conditions in Australia Amplified by Aerosol Reductions**

325 **in China**

326 The rising levels of Asian aerosols could influence the meridional temperature and pressure

327 gradients across the Indian Ocean and therefore affect monsoonal winds and rainfall in Australia

328 since the middle of the 20th century, as reported in several previous studies (Fahrenbach et al.,

329 2023; Rotstayn et al., 2007). Since 2013, aerosol levels in China have substantially decreased due

330 to clean air actions initiated by the Chinese government (Zhang et al., 2019). At the same time,

331 precipitation in Australia exhibited a declining trend, which could be partly attributed to the

332 decrease in China's anthropogenic aerosol forcing as quantified through CESM1 simulations.

333 Asian monsoon region is closely connected with the meridional Hadley circulation and zonal

334 Walker circulation through monsoon outflow to the South India ocean subtropical high (SISH) and

335 North Pacific subtropical high (NPSH) (Beck et al., 2018). Figure ~~S16~~4a illustrates the

336 climatological mean wind fields at 850 hPa, indicating the persistent existence of SISH in the

337 Indian Ocean and NPSH in the North Pacific. With reductions in aerosols in China, the sea surface

338 temperature (SST) increases in the North Pacific but decreases in the Indian Ocean (Fig. ~~S17~~4b),

339 which is concurrent with the northward shift of the Intertropical Convergence Zone (ITCZ) (Basha

340 et al., 2015). Over Asia, this migration of ITCZ is accompanied by the northward movement of

341 the upper-tropospheric subtropical zonal westerly jet (Chiang et al., 2015; Schiemann et al., 2009),

342 which moves to the north of the Tibetan Plateau. It then enhances the circulation pattern of the

343 Tibetan high, redirects the outflow from the Asian monsoon to the southern Indian Ocean

344 subtropical high (Fig. ~~3e~~5c), strengthens the SISH, and leads to the enhancement of the Southern

345 Trade Winds (Fig. ~~3d~~5d). On the other hand, the increase in SST in the North Pacific induces

346 ascending motion around the 130°–150°E and the subsequent descending motion around the 90°–

347 110°E (Fig. ~~3b~~5b), with anomalous westerly winds near the surface, leading to a weakening of

348 NPSH along with a decrease in the Northern Trade Winds (Fig. ~~3d~~5d). Note that, the descending

349 motion partly compensates the ascending motion related to the meridional circulation between

350 10°–30°N (Fig. ~~3c). Similar changes of vertical and horizontal circulations are also shown in the~~

351 ~~real world in the 2010s (Fig.~~ 5c). The mechanism of China's aerosol reductions on the large-scale

352 3D circulation in the Asia-Pacific region is shown in Figure 6.~~S18).~~ The enhancement of the

353 Southern Trade Winds further causes moisture advection away from Australia, accompanied by

354 moisture divergence in Australia, especially over the northern Australia (Fig. S18).~~S19). Moisture~~

355 ~~divergence is also evident in the observations for some northern regions of Australia (Fig. S20).~~

356 This moisture divergence in Australia then intensifies the dryness in Australia ~~both in CESM1~~

357 ~~simulations~~ (Fig. 1~~) and ERA5 reanalysis (Fig. 2~~).

358 Figures ~~S21~~7 illustrate the changes in relevant radiative fluxes in Australia resulting from

359 aerosol changes in China. Under the clear sky condition, both surface and top of the atmosphere

360 (TOA) radiative flux decrease (Fig. ~~S21e~~7c&d). It is due to increased sea salt and dust aerosols

361 (Fig. ~~S22b~~S19b–d) due to the stronger Southern Trade Winds (Figs. ~~S22a~~S19a and ~~3d~~5d) and dryer

362 conditions (Fig. ~~1a&e~~1). The decrease in cloud cover (Fig. ~~S12~~S17) leads to an overall increase in

363 both surface and TOA radiative flux (Fig. ~~S21e~~7e&f). The overall changes in radiative fluxes are

364 offset by these two factors (Fig. ~~S21a~~7a&b) and insufficient to explain the significant increase in

365 surface air temperature in Australia (Fig. ~~1b). Similar signals are also evident in the observational~~

366 ~~data represented by ERA5 and CERES-EBAF (Figs. S23 and S24~~1).

367 Decreases in precipitation lead to a decrease in surface specific humidity (Fig. ~~S25a~~S20a),

368 which declines more than that at 850 hPa (Fig. ~~S25b~~S20b). This results in excess energy being

369 converted into sensible heat rather than latent heat through evaporation (Chiang et al., 2018;

370 Fischer et al., 2007; Seneviratne et al., 2006; Su et al., 2014), which is indicated by a decrease in

371 surface upward latent heat flux and an increase in surface upward sensible heat flux in Australia

372 due to aerosol changes in China in Figure ~~S26~~8. The increased surface upward sensible heat flux

373 heats the near-surface air and contributes to the warm conditions in Australia. ~~The signals of~~

374 ~~specific humidity and surface sensible/latent heat flux from ERA5 are consistent with the~~

375 ~~simulated results. (Figs. S27 and S28).~~

3.3 Increases in Wildfire Risk in Australia

377 Wildfires represent a biosphere-atmosphere phenomenon, arising from the intricate interplay

378 of weather, climate, fuels, and human activities (Moritz et al., 2014). Notably, wildfires are ranked

379 among the most significant natural disasters in Australia, causing extensive damage (Shi et al.,

380 2021). Collins et al. (2022) reported that warmer and drier conditions increased the potential for

381 large and severe wildfire in Australia. Given that changes in aerosols in China have led to a warmer

382 and drier climate condition in Australia in recent years, the change in this climate state could also

383 impact on the occurrence of wildfires. Three wildfire risk indices (ET_0, VPD, and FFDI) are

384 selected to assess the risks of wildfires occurrence. Detailed information about the three wildfire

385 risk indices can be found in the Methods section.

386 All three indices exhibit increases (+0.37 mm mon^{-1} for ET_0, +0.56 hPa for VPD, and +0.25

387 for FFDI) during fire seasons (September to February) in Australia due to changes in aerosols in

388 China during 2013–2019 (Fig. ~~4~~9), although they do not show the same spatial distribution

389 possibly due to different considerations regarding climate variables in the indices. ~~The results~~

390 ~~analyzed from observational data also exhibit increasing trends at a rate of 0.32 mm mon^{-1} yr^{-1} for~~

391 ~~ET_0, 0.59 hPa yr^{-1} for VPD, and 0.34 yr^{-1} for FFDI during this time period (Fig. S29). It further~~

392 ~~indicates that the decline in anthropogenic aerosols in China can explain 12%–19% of the increase~~

393 ~~in wildfire risks during the fire season in Australia between 2013 and 2019 through inducing dry~~
394 ~~and warm wildfire weather conditions (Fig. S9).~~

4 Conclusions and Discussions

396   This study reveals a plausible connection between the substantial aerosol reduction in China
397 and drying and warming trends in Australia that happened during the 2010s. Aerosol reductions in
398 China induce changes in temperature and pressure gradients, which lead to an increased outflow
399 from Asia towards the South Indian Ocean, strengthening the SISH and the associated Southern
400 Trade Winds. Consequently, this atmospheric pattern results in moisture divergence over Australia,
401 causing a decrease in humidity and precipitation. The reduction in surface moisture leads to more
402 surface energy being converted into sensible heat, rather than evaporating as latent heat, thereby
403 heating the near-surface air. This perspective sheds light on the influence of distant aerosols on
404 climate in Australia.

405   The CESM1 simulations depict warmer and drier conditions in Australia related to China's
406 aerosol reductions than otherwise, a pattern also evident in observations represented by ERA5.
407 However, it is important to note that China's aerosol reductions only contribute to a portion of the
408 observed warm and dry conditions in Australia. ~~According to the CESM1 simulations, aerosol~~
409 ~~changes in China account for 19% of the observed decrease in relative humidity and precipitation~~
410 ~~and 8% of the increase in temperature in Australia throughout the year, and 12% 19% of the~~
411 ~~increase in wildfire risks during the fire season in Australia during 2013 2019.~~ Nonetheless, air
412 quality and human health improvements owing to aerosol reductions cannot be ignored (Giani et
413 al., 2020; Zheng et al., 2017). In addition, the drying and warming trends in Australia attributed to
414 aerosol reductions should be considered resulting from the rise in long-lived GHGs, while the
415 aerosol reductions unmask the effect rooted in the GHGs (Wang et al., 2023). In addition, other
416 factors such as internal climate variability (Heidemann et al., 2023) appear to have contributed
417 more to the changes in Australia's climate conditions.

418   Rotstayn et al. (2007) and Fahrenbach et al. (2023) investigated the impact of increasing
419 anthropogenic aerosols over Asia during the late 20th century and early 21st century and indicated
420 that enhanced aerosol emissions strengthened the meridional temperature and pressure gradients,
421 intensifying the monsoonal circulation and leading to increased precipitation over Australia. In

422   contrast, our study focuses on the recent reductions in anthropogenic aerosols in China since 2013,

423   showing that the aerosol reductions reversed circulation changes induced by the previous aerosol

424   increases and contributed to drying rather than increased rainfall over Australia. Our study also

425   explores the subsequent impact of aerosol reductions in China on Australian temperature. We find

426   that reduced moisture availability over Australia led to a shift in surface energy partitioning, with

427   more energy being converted into sensible heat rather than latent heat, resulting in near-surface

428   warming. In summary, while previous studies have demonstrated the role of increasing Asian

429   aerosols in enhancing Australia's precipitation, our work complements these findings by showing

430   that decreasing aerosols, particularly from China, can drive the opposite effect, contributing to

431   both drying and warming conditions in Australia.

432   One limitation of this study is the use of equilibrium experiments. Although the equilibrium

433   method is useful for isolating aerosol-induced climate responses, it does not fully capture the

434   transient climatic evolution. Attributing observed climate changes directly to modeled aerosol-

435   induced responses involves inherent uncertainties. Given the uncertainties, here we did not attempt

436   to quantitatively attribute the observed climate change to aerosols in this study, but showed the

437   mechanisms that how aerosol decline influence remote climate. Future work could also consider

438   transient simulations, which can better represent the role of aerosols in the climatic evolution of

439   the real world.

440   There are some other potential ~~limitations and~~ uncertainties in this study. Firstly, the low bias

441   in simulated aerosol concentrations in CESM1 ~~could potentially lead to an underestimation of the~~

442   ~~climate responses in Australia, and the extent to which the low bias~~ and CESM1's larger sensitivity

443   to aerosol forcing could ~~influence the results remains unknown.~~ introduce some uncertainties.

444   Secondly, our findings are derived from simulations conducted with a single ~~aerosol~~ fully-coupled

445   climate model, and it is vital for future research to employ multi-model ensemble simulations to

446   reduce the possibility of model-dependent specific results. While the CMIP6 and PDRMIP

447   (Precipitation Driver Response Model Intercomparison Project) can assist in minimizing such

448   model dependencies, they also present certain drawbacks. Anthropogenic emissions input in

449   CMIP6 inadequately accounts for aerosol reductions resulting from clean air actions in China since

450   2013 (Z. Wang et al., 2021). Additionally, CMIP6 considers aerosol changes globally, making it

451   challenging to isolate effects specifically induced by changes in aerosols in China. The

452 experimental design of PDRMIP, which scales the concentrations of sulfate and BC in Asia to ten

453 times of their present-day levels, is generally idealistic and may not accurately and proportionally

454 represent aerosol changes observed in the real world. ~~Until now, few studies have explored the~~

455 ~~link between the recent reduction in China's aerosols and the changing climate conditions in~~

456 ~~Australia. Although Fahrenbach et al. (2023) investigated the connection between increased~~

457 ~~precipitation in Australia and elevated aerosol levels in Asia since the last century, they focused~~

458 ~~on the decadal time scale with historical increasing aerosols in Asia.~~ Finally, in addition to aerosols,

459 GHGs and nature variabilities also contribute to regional and global climate change. The extent to

460 which GHGs and nature variabilities could contribute to weather condition and climate changes in

461 Australia remains unknown, which warrants further investigation.

462 Nonetheless, our study examined the role of China's aerosol reductions in Australia's recent

463 drying and warming trends. Substantial emission reductions will continue in China following the

464 carbon neutral pathway (Yang et al., 2023), while future changes in emissions in South Asia remain

465 uncertain (Samset et al., 2019). Apart from natural climate variabilities that affect the Australian

466 monsoon, further investigation of changes in monsoon precipitation in Australia should also

467 consider the effects of remote aerosol changes simultaneously, which is crucial to effective drought

468 and wildfire management and mitigation in Australia.

Acknowledgments

470 This study was supported by the National Natural Science Foundation of China (grant no.

471 42475032), the Jiangsu Science Fund for Carbon Neutrality (grant no. BK20220031), and Jiangsu

472 Innovation and Entrepreneurship Team (grant no. JSSCTD202346). H.W. acknowledges the

473 support of the U.S. Department of Energy (DOE), Office of Science, Office of Biological and

474 Environmental Research (BER), as part of the Earth and Environmental System Modeling program.

475 The Pacific Northwest National Laboratory (PNNL) is operated for DOE by the Battelle Memorial

476 Institute under contract DE-AC05-76RLO1830.

Data and Code Availability

478 Ground-based observed $PM_{2.5}$ concentrations from CNEMC are available at

479 https://quotsoft.net/air/ (last access: September 2024). AOD from MODIS Deep Blue retrieval are

480 available at https://modis.gsfc.nasa.gov/ (last access: September 2024). ERA5 reanalysis data are

481 available at https://cds.climate.copernicus.eu/ (last access: September 2024). ~~CERES EBAF data~~

482 ~~are available at https://ceres.larc.nasa.gov/data/#energy-balanced-and-filled-ebaf (last access:~~

483 ~~September 2024).~~ GPM data are available at

484 https://disc.gsfc.nasa.gov/datasets/GPM_3IMERGM_07/summary?keywords=%22IMERG%20fi

485 nal%22 (last access: September 2024). GPCP data are available at

486 https://psl.noaa.gov/data/gridded/data.gpcp.html (last access: April 2025). The source code of

487 CESM is available at https://github.com/ESCOMP/CESM (last access: September 2024). Our

488 model results can be available at https://doi.org/10.5281/zenodo.13682943 (last access: September

489 2024).

Author Contributions

491 Y.Y. conceived the research and directed the analysis. J.G. conceived the research, conducted

492 the model simulations, and performed the analysis. All the authors including H.W., P.W., and H.

493 L. discussed the results and wrote the paper.

Competing Interests

495 At least one of the (co-)authors is a member of the editorial board of Atmospheric Chemistry

496 and Physics. The peer-review process was guided by an independent editor, and the authors also

497 have no other competing interests to declare.

References

499 Adler, R., Sapiano, M., Huffman, G., Wang, J.-J., Gu, G., Bolvin, D., Chiu, L., Schneider, U.,
500   Becker, A., Nelkin, E., Xie, P., Ferraro, R., and Shin, D.-B.: The Global Precipitation
501   Climatology Project (GPCP) Monthly Analysis (New Version 2.3) and a Review of 2017
502   Global Precipitation, Atmosphere, 9, 138, https://doi.org/10.3390/atmos9040138, 2018.

503 Basha, G., Kishore, P., Venkat Ratnam, M., Ouarda, T. B. M. J., Velicogna, I., and Sutterley, T.:
504   Vertical and latitudinal variation of the intertropical convergence zone derived using GPS
505   radio occultation measurements, Remote Sens. Environ., 163, 262–269,
506   https://doi.org/10.1016/j.rse.2015.03.024, 2015.

507 Beck, J. W., Zhou, W., Li, C., Wu, Z., White, L., Xian, F., Kong, X., and An, Z.: A 550,000-year
508   record of East Asian monsoon rainfall from 10Be in loess, Science, 360, 877–881,
509   https://doi.org/10.1126/science.aam5825, 2018.

510 Boer, M. M., Resco De Dios, V., and Bradstock, R. A.: Unprecedented burn area of Australian
511   mega forest fires, Nat. Clim. Change, 10, 171–172, https://doi.org/10.1038/s41558-020-
512   0716-1, 2020.

513 Bollasina, M. A., Ming, Y., and Ramaswamy, V.: Anthropogenic Aerosols and the Weakening of
514   the South Asian Summer Monsoon, Science, 334, 502–505,
515   https://doi.org/10.1126/science.1204994, 2011.

516 Bollasina, M. A., Ming, Y., Ramaswamy, V., Schwarzkopf, M. D., and Naik, V.: Contribution of
517   local and remote anthropogenic aerosols to the twentieth century weakening of the South
518   Asian Monsoon, Geophys. Res. Lett., 41, 680–687, https://doi.org/10.1002/2013GL058183,
519   2014.

520 Chiang, F., Mazdiyasni, O., and AghaKouchak, A.: Amplified warming of droughts in southern
521   United States in observations and model simulations, Sci. Adv., 4, eaat2380,
522   https://doi.org/10.1126/sciadv.aat2380, 2018.

523 Chiang, J. C. H., Fung, I. Y., Wu, C.-H., Cai, Y., Edman, J. P., Liu, Y., Day, J. A., Bhattacharya,
524   T., Mondal, Y., and Labrousse, C. A.: Role of seasonal transitions and westerly jets in East
525   Asian paleoclimate, Quat. Sci. Rev., 108, 111–129,
526   https://doi.org/10.1016/j.quascirev.2014.11.009, 2015.

527 Collins, L., Clarke, H., Clarke, M. F., McColl Gausden, S. C., Nolan, R. H., Penman, T., and
528   Bradstock, R.: Warmer and drier conditions have increased the potential for large and severe
529   fire seasons across south-eastern Australia, Glob. Ecol. Biogeogr., 31, 1933–1948,
530   https://doi.org/10.1111/geb.13514, 2022.

531 Cook, B. I. and Seager, R.: The response of the North American Monsoon to increased greenhouse
532   gas forcing, J. Geophys. Res.: Atmos., 118, 1690–1699, https://doi.org/10.1002/jgrd.50111,
533   2013.

534 Cowan, T. and Cai, W.: The impact of Asian and non-Asian anthropogenic aerosols on 20th
535   century Asian summer monsoon: ASIAN MONSOON AND AEROSOLS, Geophys. Res.
536   Lett., 38, L11703, https://doi.org/10.1029/2011GL047268, 2011.

537 CSIRO and BOM: State of the Climate 2022, 2022

538 Dang, R. and Liao, H.: Radiative Forcing and Health Impact of Aerosols and Ozone in China as
539   the Consequence of Clean Air Actions over 2012–2017, Geophys. Res. Lett., 46, 12511–
540   12519, https://doi.org/10.1029/2019GL084605, 2019.

541 Dey, R., Lewis, S. C., Arblaster, J. M., and Abram, N. J.: A review of past and projected changes
542   in Australia's rainfall, WIREs Clim. Change, 10, e577, https://doi.org/10.1002/wcc.577,
543   2019a.

544 Dey, R., Lewis, S. C., and Abram, N. J.: Investigating observed northwest Australian rainfall
545   trends in Coupled Model Intercomparison Project phase 5 detection and attribution
546   experiments, Int. J. Climatol., 39, 112–127, https://doi.org/10.1002/joc.5788, 2019b.

Dong, B., Wilcox, L. J., Highwood, E. J., and Sutton, R. T.: Impacts of recent decadal changes in Asian aerosols on the East Asian summer monsoon: roles of aerosol–radiation and aerosol–cloud interactions, Clim. Dyn., 53, 3235–3256, https://doi.org/10.1007/s00382-019-04698-0, 2019.

Dowdy, A. J.: Seamless climate change projections and seasonal predictions for bushfires in Australia, J. South. Hemisph. Earth Syst. Sci., 70, 120–138, https://doi.org/10.1071/ES20001, 2020.

Evans, S., Marchand, R., and Ackerman, T.: Variability of the Australian Monsoon and Precipitation Trends at Darwin, J. Climate, 27, 8487–8500, https://doi.org/10.1175/JCLI-D-13-00422.1, 2014.

Fahrenbach, N. L. S., Bollasina, M. A., Samset, B. H., Cowan, T., and Ekman, A. M. L.: Asian anthropogenic aerosol forcing played a key role in the multi-decadal increase in Australian summer monsoon rainfall, J. Climate, 1, https://doi.org/10.1175/JCLI-D-23-0313.1, 2023.

Fan, T., Liu, X., Ma, P.-L., Zhang, Q., Li, Z., Jiang, Y., Zhang, F., Zhao, C., Yang, X., Wu, F., and Wang, Y.: Emission or atmospheric processes? An attempt to attribute the source of large bias of aerosols in eastern China simulated by global climate models, Atmos. Chem. Phys., 18, 1395–1417, https://doi.org/10.5194/acp-18-1395-2018, 2018.

Fan, T., Liu, X., Wu, C., Zhang, Q., Zhao, C., Yang, X., and Li, Y.: Comparison of the Anthropogenic Emission Inventory for CMIP6 Models with a Country-Level Inventory over China and the Simulations of the Aerosol Properties, Adv. Atmos. Sci., 39, 80–96, https://doi.org/10.1007/s00376-021-1119-6, 2022.

Fischer, E. M., Seneviratne, S. I., Lüthi, D., and Schär, C.: Contribution of land-atmosphere coupling to recent European summer heat waves, Geophys. Res. Lett., 34, 2006GL029068, https://doi.org/10.1029/2006GL029068, 2007.

Gao, J., Yang, Y., Wang, H., Wang, P., Li, H., Li, M., Ren, L., Yue, X., and Liao, H.: Fast climate responses to emission reductions in aerosol and ozone precursors in China during 2013–2017, Atmos. Chem. Phys., 22, 7131–7142, https://doi.org/10.5194/acp-22-7131-2022, 2022.

Gao, J., Yang, Y., Wang, H., Wang, P., Li, B., Li, J., Wei, J., Gao, M., and Liao, H.: Climate responses in China to domestic and foreign aerosol changes due to clean air actions during 2013–2019, npj Clim. Atmos. Sci., 6, 160, https://doi.org/10.1038/s41612-023-00488-y, 2023.

Giani, P., Castruccio, S., Anav, A., Howard, D., Hu, W., and Crippa, P.: Short-term and long-term health impacts of air pollution reductions from COVID-19 lockdowns in China and Europe: a modelling study, Lancet Planet. Health, 4, e474–e482, https://doi.org/10.1016/S2542-5196(20)30224-2, 2020.

Guenther, A. B., Jiang, X., Heald, C. L., Sakulyanontvittaya, T., Duhl, T., Emmons, L. K., and Wang, X.: The Model of Emissions of Gases and Aerosols from Nature version 2.1

585   (MEGAN2.1): an extended and updated framework for modeling biogenic emissions, Geosci.
586   Model Dev., 5, 1471–1492, https://doi.org/10.5194/gmd-5-1471-2012, 2012.

587 He, T., Lamont, B. B., and Pausas, J. G.: Fire as a key driver of Earth's biodiversity, Biol. Rev.,
588   94, 1983–2010, https://doi.org/10.1111/brv.12544, 2019.

589 Head, L., Adams, M., McGregor, H. V., and Toole, S.: Climate change and Australia, WIREs Clim.
590   Change, 5, 175–197, https://doi.org/10.1002/wcc.255, 2014.

591 Heidemann, H., Cowan, T., Henley, B. J., Ribbe, J., Freund, M., and Power, S.: Variability and
592   long-term change in Australian monsoon rainfall: A review, WIREs Clim. Change, 14, e823,
593   https://doi.org/10.1002/wcc.823, 2023.

594 Hersbach, H., Bell, B., Berrisford, P., Hirahara, S., Horányi, A., Muñoz-Sabater, J., Nicolas, J.,
595   Peubey, C., Radu, R., Schepers, D., Simmons, A., Soci, C., Abdalla, S., Abellan, X., Balsamo,
596   G., Bechtold, P., Biavati, G., Bidlot, J., Bonavita, M., De Chiara, G., Dahlgren, P., Dee, D.,
597   Diamantakis, M., Dragani, R., Flemming, J., Forbes, R., Fuentes, M., Geer, A., Haimberger,
598   L., Healy, S., Hogan, R. J., Hólm, E., Janisková, M., Keeley, S., Laloyaux, P., Lopez, P.,
599   Lupu, C., Radnoti, G., De Rosnay, P., Rozum, I., Vamborg, F., Villaume, S., and Thépaut, J.:
600   The ERA5 global reanalysis, Q. J. R. Meteorol. Soc., 146, 1999–2049,
601   https://doi.org/10.1002/qj.3803, 2020.

602 Hoesly, R. M., Smith, S. J., Feng, L., Klimont, Z., Janssens-Maenhout, G., Pitkanen, T., Seibert,
603   J. J., Vu, L., Andres, R. J., Bolt, R. M., Bond, T. C., Dawidowski, L., Kholod, N., Kurokawa,
604   J., Li, M., Liu, L., Lu, Z., Moura, M. C. P., O'Rourke, P. R., and Zhang, Q.: Historical (1750–
605   2014) anthropogenic emissions of reactive gases and aerosols from the Community Emissions
606   Data System (CEDS), Geosci. Model Dev., 11, 369–408, https://doi.org/10.5194/gmd-11-
607   369-2018, 2018.

608 Hsu, N. C., Jeong, M. -J., Bettenhausen, C., Sayer, A. M., Hansell, R., Seftor, C. S., Huang, J., and
609   Tsay, S. -C.: Enhanced Deep Blue aerosol retrieval algorithm: The second generation, J.
610   Geophys. Res.: Atmos., 118, 9296–9315, https://doi.org/10.1002/jgrd.50712, 2013.

611 Huneeus, N., Denier Van Der Gon, H., Castesana, P., Menares, C., Granier, C., Granier, L., Alonso,
612   M., De Fatima Andrade, M., Dawidowski, L., Gallardo, L., Gomez, D., Klimont, Z., Janssens-
613   Maenhout, G., Osses, M., Puliafito, S. E., Rojas, N., Ccoyllo, O. S.-, Tolvett, S., and Ynoue,
614   R. Y.: Evaluation of anthropogenic air pollutant emission inventories for South America at
615   national and city scale, Atmos. Environ., 235, 117606,
616   https://doi.org/10.1016/j.atmosenv.2020.117606, 2020.

617 IPCC: Climate Change 2013: The Physical Science Basis, 2013.

618 IPCC: Climate Change 2021: The Physical Science Basis, 2021.

619 Irmak, S., Irmak, A., Allen, R. G., and Jones, J. W.: Solar and Net Radiation-Based Equations to
620   Estimate Reference Evapotranspiration in Humid Climates, J. Irrig. Drain. Eng., 129, 336–
621   347, https://doi.org/10.1061/(ASCE)0733-9437(2003)129:5(336), 2003.

622 Johnston, F. H., Borchers-Arriagada, N., Morgan, G. G., Jalaludin, B., Palmer, A. J., Williamson,
623   G. J., and Bowman, D. M. J. S.: Unprecedented health costs of smoke-related PM2.5 from
624   the 2019–20 Australian megafires, Nat. Sustain., 4, 42–47, https://doi.org/10.1038/s41893-
625   020-00610-5, 2021.

626 Jones, M. W., Abatzoglou, J. T., Veraverbeke, S., Andela, N., Lasslop, G., Forkel, M., Smith, A.
627   J. P., Burton, C., Betts, R. A., van der Werf, G. R., Sitch, S., Canadell, J. G., Santín, C.,
628   Kolden, C., Doerr, S. H., and Le Quéré, C.: Global and Regional Trends and Drivers of Fire
629   Under Climate Change, Rev. Geophys., 60, e2020RG000726,
630   https://doi.org/10.1029/2020RG000726, 2022.

631 Kloster, S., Dentener, F., Feichter, J., Raes, F., Lohmann, U., Roeckner, E., and Fischer-Bruns, I.:
632   A GCM study of future climate response to aerosol pollution reductions, Clim. Dyn., 34,
633   1177–1194, https://doi.org/10.1007/s00382-009-0573-0, 2010.

634 Lau, K.-M. and Kim, K.-M.: Observational relationships between aerosol and Asian monsoon
635   rainfall, and circulation, Geophys. Res. Lett., 33, 2006GL027546,
636   https://doi.org/10.1029/2006GL027546, 2006.

637 Leibensperger, E. M., Mickley, L. J., Jacob, D. J., Chen, W.-T., Seinfeld, J. H., Nenes, A., Adams,
638   P. J., Streets, D. G., Kumar, N., and Rind, D.: Climatic effects of 1950–2050 changes in US
639   anthropogenic aerosols – Part 1: Aerosol trends and radiative forcing, Atmos. Chem. Phys.,
640   12, 3333–3348, https://doi.org/10.5194/acp-12-3333-2012, 2012.

641 Liu, C., Yang, Y., Wang, H., Ren, L., Wei, J., Wang, P., and Liao, H.: Influence of Spatial Dipole
642   Pattern in Asian Aerosol Changes on East Asian Summer Monsoon, J. Climate, 36, 1575–
643   1585, https://doi.org/10.1175/JCLI-D-22-0335.1, 2023.

644 Liu, X., Ma, P.-L., Wang, H., Tilmes, S., Singh, B., Easter, R. C., Ghan, S. J., and Rasch, P. J.:
645   Description and evaluation of a new four-mode version of the Modal Aerosol Module
646   (MAM4) within version 5.3 of the Community Atmosphere Model, Geosci. Model Dev., 9,
647   505–522, https://doi.org/10.5194/gmd-9-505-2016, 2016.

648 ~~Loeb, N. G., Doelling, D. R., Wang, H., Su, W., Nguyen, C., Corbett, J. G., Liang, L., Mitrescu,~~
649   ~~C., Rose, F. G., and Kato, S.: Clouds and the Earth's Radiant Energy System (CERES) Energy~~
650   ~~Balanced and Filled (EBAF) Top-of-Atmosphere (TOA) Edition-4.0 Data Product, J. Climate,~~
651   ~~31, 895–918, https://doi.org/10.1175/JCLI-D-17-0208.1, 2018.~~

652 Ming, Y. and Ramaswamy, V.: Nonlinear Climate and Hydrological Responses to Aerosol Effects,
653   J. Climate, 22, 1329–1339, https://doi.org/10.1175/2008JCLI2362.1, 2009.

654 Moritz, M. A., Batllori, E., Bradstock, R. A., Gill, A. M., Handmer, J., Hessburg, P. F., Leonard,
655   J., McCaffrey, S., Odion, D. C., Schoennagel, T., and Syphard, A. D.: Learning to coexist
656   with wildfire, Nature, 515, 58–66, https://doi.org/10.1038/nature13946, 2014.

657 Nicholls, N.: Detecting and attributing Australian climate change: a review, Aust. Meteorol. Mag.,
658   2006.

Oh, H. and Ha, K.-J.: Thermodynamic characteristics and responses to ENSO of dominant intraseasonal modes in the East Asian summer monsoon, Clim. Dyn., 44, 1751–1766, https://doi.org/10.1007/s00382-014-2268-4, 2015.

Pozzoli, L., Janssens-Maenhout, G., Diehl, T., Bey, I., Schultz, M. G., Feichter, J., Vignati, E., and Dentener, F.: Re-analysis of tropospheric sulfate aerosol and ozone for the period 1980–2005 using the aerosol-chemistry-climate model ECHAM5-HAMMOZ, Atmos. Chem. Phys., 11, 9563–9594, https://doi.org/10.5194/acp-11-9563-2011, 2011.

Rauniyar, S. P. and Power, S. B.: The Impact of Anthropogenic Forcing and Natural Processes on Past, Present, and Future Rainfall over Victoria, Australia, J. Climate, 33, 8087–8106, https://doi.org/10.1175/JCLI-D-19-0759.1, 2020.

Ren, L., Yang, Y., Wang, H., Wang, P., Yue, X., and Liao, H.: Widespread Wildfires Over the Western United States in 2020 Linked to Emissions Reductions During COVID-19, Geophys. Res. Lett., 49, e2022GL099308, https://doi.org/10.1029/2022GL099308, 2022.

Risbey, J. S., Pook, M. J., McIntosh, P. C., Wheeler, M. C., and Hendon, H. H.: On the Remote Drivers of Rainfall Variability in Australia, Mon. Wea. Rev., 137, 3233–3253, https://doi.org/10.1175/2009MWR2861.1, 2009.

Rotstayn, L. D., Cai, W., Dix, M. R., Farquhar, G. D., Feng, Y., Ginoux, P., Herzog, M., Ito, A., Penner, J. E., Roderick, M. L., and Wang, M.: Have Australian rainfall and cloudiness increased due to the remote effects of Asian anthropogenic aerosols?, J. Geophys. Res.: Atmos., 112, 2006JD007712, https://doi.org/10.1029/2006JD007712, 2007.

Samset, B. H., Lund, M. T., Bollasina, M., Myhre, G., and Wilcox, L.: Emerging Asian aerosol patterns, Nat. Geosci., 12, 582–584, https://doi.org/10.1038/s41561-019-0424-5, 2019.

Schiemann, R., Lüthi, D., and Schär, C.: Seasonality and Interannual Variability of the Westerly Jet in the Tibetan Plateau Region, J. Climate, 22, 2940–2957, https://doi.org/10.1175/2008JCLI2625.1, 2009.

Seager, R., Hooks, A., Williams, A. P., Cook, B., Nakamura, J., and Henderson, N.: Climatology, Variability, and Trends in the U.S. Vapor Pressure Deficit, an Important Fire-Related Meteorological Quantity, J. Appl. Meteorol. Clim., 54, 1121–1141, https://doi.org/10.1175/JAMC-D-14-0321.1, 2015.

Seneviratne, S. I., Lüthi, D., Litschi, M., and Schär, C.: Land–atmosphere coupling and climate change in Europe, Nature, 443, 205–209, https://doi.org/10.1038/nature05095, 2006.

Sharples, J. J., McRae, R. H. D., Weber, R. O., and Gill, A. M.: A simple index for assessing fire danger rating, Environ. Modell. Softw., 24, 764–774, https://doi.org/10.1016/j.envsoft.2008.11.004, 2009.

Shi, G., Yan, H., Zhang, W., Dodson, J., Heijnis, H., and Burrows, M.: Rapid warming has resulted in more wildfires in northeastern Australia, Sci. Total Environ., 771, 144888, https://doi.org/10.1016/j.scitotenv.2020.144888, 2021.

Skofronick-Jackson, G., Petersen, W. A., Berg, W., Kidd, C., Stocker, E. F., Kirschbaum, D. B., Kakar, R., Braun, S. A., Huffman, G. J., Iguchi, T., Kirstetter, P. E., Kummerow, C., Meneghini, R., Oki, R., Olson, W. S., Takayabu, Y. N., Furukawa, K., and Wilheit, T.: The Global Precipitation Measurement (GPM) Mission for Science and Society, Bull. Am. Meteorol. Soc., 98, 1679–1695, https://doi.org/10.1175/BAMS-D-15-00306.1, 2017.

Streets, D. G., Yan, F., Chin, M., Diehl, T., Mahowald, N., Schultz, M., Wild, M., Wu, Y., and Yu, C.: Anthropogenic and natural contributions to regional trends in aerosol optical depth, 1980–2006, J. Geophys. Res.: Atmos., 114, 2008JD011624, https://doi.org/10.1029/2008JD011624, 2009.

Su, H., Yang, Z., Dickinson, R. E., and Wei, J.: Spring soil moisture-precipitation feedback in the Southern Great Plains: How is it related to large-scale atmospheric conditions?, Geophys. Res. Lett., 41, 1283–1289, https://doi.org/10.1002/2013GL058931, 2014.

Turnock, S. T., Allen, R. J., Andrews, M., Bauer, S. E., Deushi, M., Emmons, L., Good, P., Horowitz, L., John, J. G., Michou, M., Nabat, P., Naik, V., Neubauer, D., O'Connor, F. M., Olivié, D., Oshima, N., Schulz, M., Sellar, A., Shim, S., Takemura, T., Tilmes, S., Tsigaridis, K., Wu, T., and Zhang, J.: Historical and future changes in air pollutants from CMIP6 models, Atmos. Chem. Phys., 20, 14547–14579, https://doi.org/10.5194/acp-20-14547-2020, 2020.

Undorf, S., Polson, D., Bollasina, M. A., Ming, Y., Schurer, A., and Hegerl, G. C.: Detectable Impact of Local and Remote Anthropogenic Aerosols on the 20th Century Changes of West African and South Asian Monsoon Precipitation, J. Geophys. Res.: Atmos., 123, 4871–4889, https://doi.org/10.1029/2017JD027711, 2018.

Van Marle, M. J. E., Kloster, S., Magi, B. I., Marlon, J. R., Daniau, A.-L., Field, R. D., Arneth, A., Forrest, M., Hantson, S., Kehrwald, N. M., Knorr, W., Lasslop, G., Li, F., Mangeon, S., Yue, C., Kaiser, J. W., and Van Der Werf, G. R.: Historic global biomass burning emissions for CMIP6 (BB4CMIP) based on merging satellite observations with proxies and fire models (1750–2015), Geosci. Model Dev., 10, 3329–3357, https://doi.org/10.5194/gmd-10-3329-2017, 2017.

Wang, B., Biasutti, M., Byrne, M. P., Castro, C., Chang, C.-P., Cook, K., Fu, R., Grimm, A. M., Ha, K.-J., Hendon, H., Kitoh, A., Krishnan, R., Lee, J.-Y., Li, J., Liu, J., Moise, A., Pascale, S., Roxy, M. K., Seth, A., Sui, C.-H., Turner, A., Yang, S., Yun, K.-S., Zhang, L., and Zhou, T.: Monsoons Climate Change Assessment, Bull. Am. Meteorol. Soc., 102, E1–E19, https://doi.org/10.1175/BAMS-D-19-0335.1, 2021.

Wang, H., Easter, R. C., Rasch, P. J., Wang, M., Liu, X., Ghan, S. J., Qian, Y., Yoon, J.-H., Ma, P.-L., and Vinoj, V.: Sensitivity of remote aerosol distributions to representation of cloud–aerosol interactions in a global climate model, Geosci. Model Dev., 6, 765–782, https://doi.org/10.5194/gmd-6-765-2013, 2013.

Wang, P., Yang, Y., Xue, D., Ren, L., Tang, J., Leung, L. R., and Liao, H.: Aerosols overtake greenhouse gases causing a warmer climate and more weather extremes toward carbon neutrality, Nat. Commun., 14, 7257, https://doi.org/10.1038/s41467-023-42891-2, 2023.

Wang, Z., Zhang, H., and Zhang, X.: Projected response of East Asian summer monsoon system to future reductions in emissions of anthropogenic aerosols and their precursors, Clim. Dyn., 47, 1455–1468, https://doi.org/10.1007/s00382-015-2912-7, 2016.

Wang, Z., Lin, L., Xu, Y., Che, H., Zhang, X., Zhang, H., Dong, W., Wang, C., Gui, K., and Xie, B.: Incorrect Asian aerosols affecting the attribution and projection of regional climate change in CMIP6 models, npj Clim. Atmos. Sci., 4, 2, https://doi.org/10.1038/s41612-020-00159-2, 2021.

Ward, M., Tulloch, A. I. T., Radford, J. Q., Williams, B. A., Reside, A. E., Macdonald, S. L., Mayfield, H. J., Maron, M., Possingham, H. P., Vine, S. J., O'Connor, J. L., Massingham, E. J., Greenville, A. C., Woinarski, J. C. Z., Garnett, S. T., Lintermans, M., Scheele, B. C., Carwardine, J., Nimmo, D. G., Lindenmayer, D. B., Kooyman, R. M., Simmonds, J. S., Sonter, L. J., and Watson, J. E. M.: Impact of 2019–2020 mega-fires on Australian fauna habitat, Nat. Ecol. Evol., 4, 1321–1326, https://doi.org/10.1038/s41559-020-1251-1, 2020.

Wasko, C., Shao, Y., Vogel, E., Wilson, L., Wang, Q. J., Frost, A., and Donnelly, C.: Understanding trends in hydrologic extremes across Australia, J. Hydrol., 593, 125877, https://doi.org/10.1016/j.jhydrol.2020.125877, 2021.

Yang, Y., Zeng, L., Wang, H., Wang, P., and Liao, H.: Climate effects of future aerosol reductions for achieving carbon neutrality in China, Sci. Bull., 68, 902–905, https://doi.org/10.1016/j.scib.2023.03.048, 2023.

Zacharakis, I. and Tsihrintzis, V. A.: Integrated wildfire danger models and factors: A review, Sci. Total Environ., 899, 165704, https://doi.org/10.1016/j.scitotenv.2023.165704, 2023.

Zeng, L., Yang, Y., Wang, H., Wang, J., Li, J., Ren, L., Li, H., Zhou, Y., Wang, P., and Liao, H.: Intensified modulation of winter aerosol pollution in China by El Niño with short duration, Atmos. Chem. Phys., 21, 10745–10761, https://doi.org/10.5194/acp-21-10745-2021, 2021.

Zhang, Q., Zheng, Y., Tong, D., Shao, M., Wang, S., Zhang, Y., Xu, X., Wang, J., He, H., Liu, W., Ding, Y., Lei, Y., Li, J., Wang, Z., Zhang, X., Wang, Y., Cheng, J., Liu, Y., Shi, Q., Yan, L., Geng, G., Hong, C., Li, M., Liu, F., Zheng, B., Cao, J., Ding, A., Gao, J., Fu, Q., Huo, J., Liu, B., Liu, Z., Yang, F., He, K., and Hao, J.: Drivers of improved PM2.5 air quality in China from 2013 to 2017, Proc. Natl. Acad. Sci., 116, 24463–24469, https://doi.org/10.1073/pnas.1907956116, 2019.

Zheng, B., Tong, D., Li, M., Liu, F., Hong, C., Geng, G., Li, H., Li, X., Peng, L., Qi, J., Yan, L., Zhang, Y., Zhao, H., Zheng, Y., He, K., and Zhang, Q.: Trends in China's anthropogenic emissions since 2010 as the consequence of clean air actions, Atmos. Chem. Phys., 18, 14095–14111, https://doi.org/10.5194/acp-18-14095-2018, 2018.

Zheng, Y., Xue, T., Zhang, Q., Geng, G., Tong, D., Li, X., and He, K.: Air quality improvements and health benefits from China's clean air action since 2013, Environ. Res. Lett., 12, 114020, https://doi.org/10.1088/1748-9326/aa8a32, 2017.

772   Zheng, Y., Zhang, Q., Tong, D., Davis, S. J., and Caldeira, K.: Climate effects of China's efforts
773   to improve its air quality, Environ. Res. Lett., 15, 104052, https://doi.org/10.1088/1748-
774   9326/ab9e21, 2020.
775

776

777   **Figure 1.**
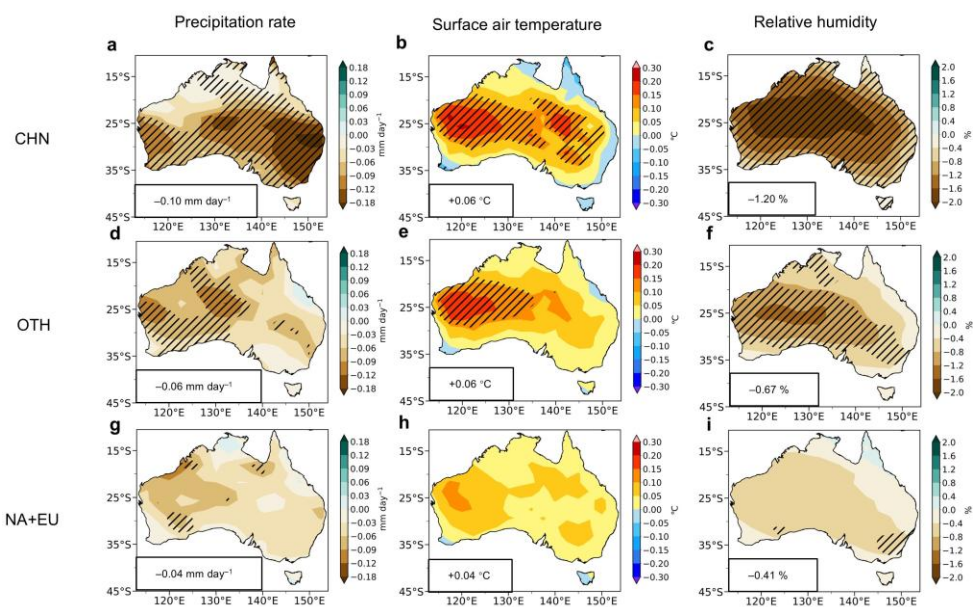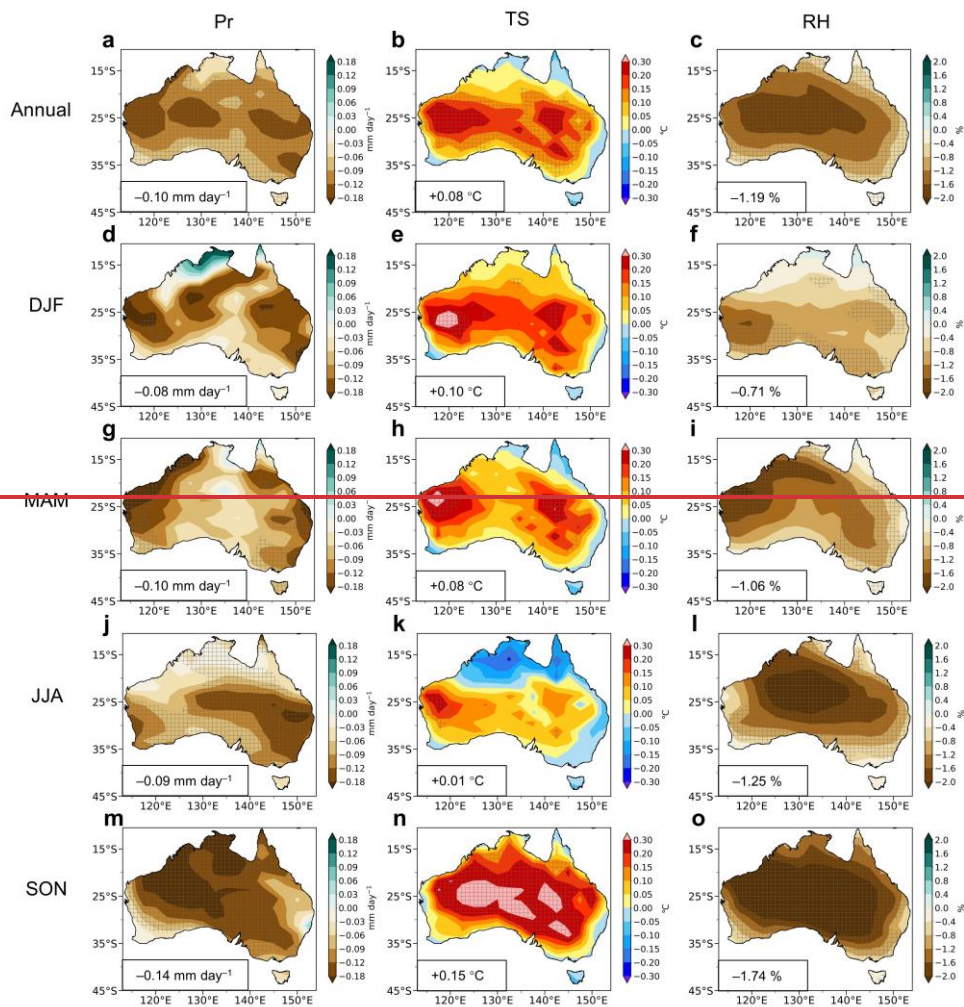
778 **Figure 1. Simulated changes in precipitation rate, surface air temperature and relative**

779 **humidity in Australia due to aerosol changes between 2013 and 2019.** Spatial distributions of

780 simulated differences in annual mean precipitation rate (Pr, **a**, **d**, and **g**, unit: mm day^{-1}), surface

781 air temperature (TS, **b**, **e**, and **h**, unit: °C) and relative humidity (RH, **c**, **f**, and **i**, unit: %) in

782 Australia between BASE and CHN (CHN minus BASE, **a**–**c**), between BASE and OTH (OTH

783 minus BASE, **d**–**f**), and between BASE and NAEU (NAEU minus BASE, **g**–**i**). The shaded areas

784 indicate results are statistically significant at the 90% confidence level. Regional averages over

785 Australia are noted at the bottom-left corner of each panel.

786
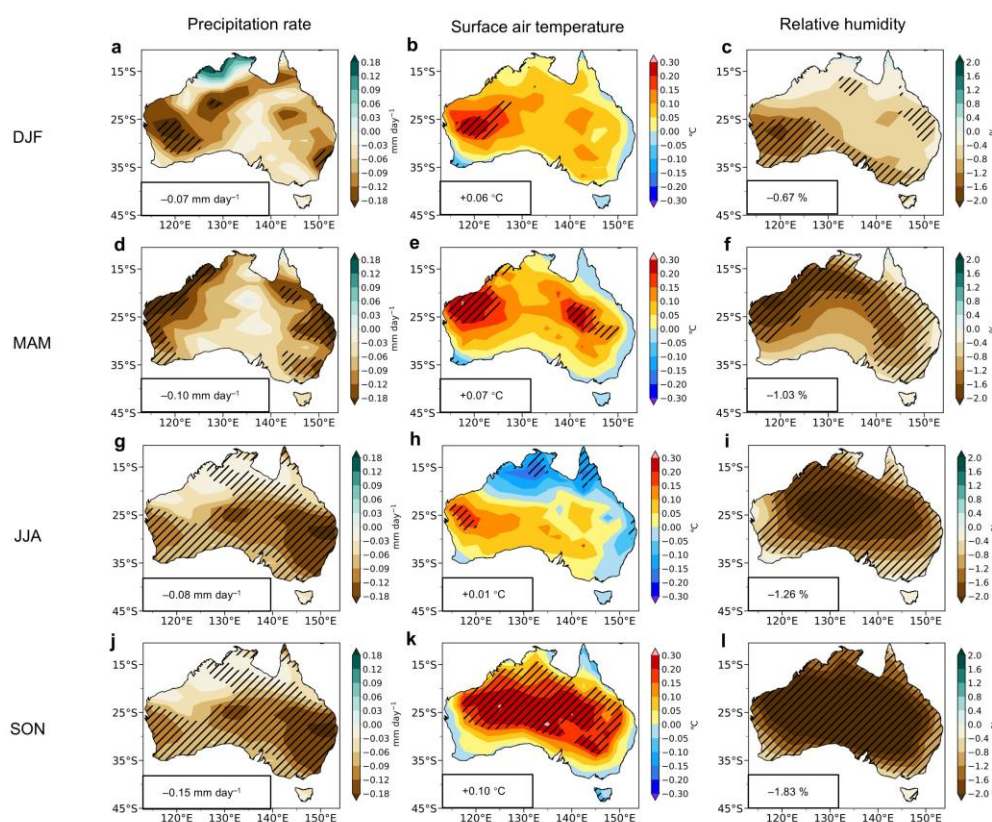
787 **Figure 2.** **Simulated changes in precipitation rate, surface air temperature and relative**

788 **humidity in Australia due to aerosol changes in China between 2013 and 2019.** Spatial

789 distributions of simulated differences in ~~annual (a–c),~~ DJF (~~d–f,~~ December, January and

790 February, **a**–**c**), MAM (~~g–I,~~ March, April and May, **d**–**f**), JJA (~~j–l,~~ June, July and August, **g**–**i**)

791 and SON (~~m–o,~~ September, October and November, **j**–**l**) mean precipitation rate (Pr, **a**, **d**, **g**, ~~j,~~

792 and ~~m~~**j**, unit: mm day^{-1}), surface air temperature (TS, **b**, **e**, **h**, ~~k,~~ and ~~n~~**k**, unit: °C) and relative

793   humidity (RH, **c**, **f**, **i**, ~~l,~~ and ~~o~~l, unit: %) in Australia between BASE and CHN (CHN minus

794   BASE). The shaded areas indicate results are statistically significant at the 90% confidence level.

795   Regional averages over Australia are noted at the bottom-left corner of each panel.

796
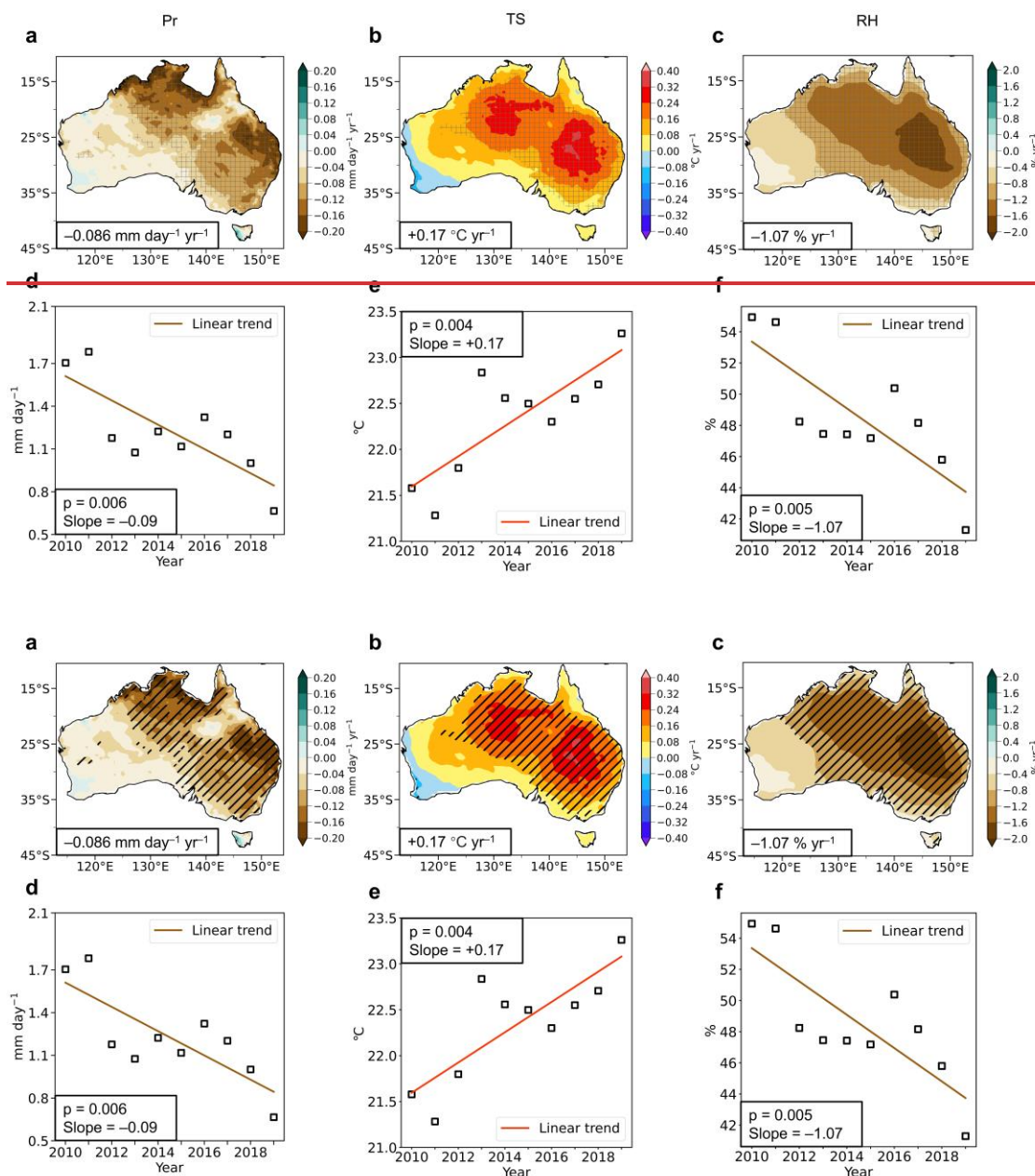
Figure ~~2~~3. Linear trends of observed precipitation rate, surface air temperature and relative humidity in Australia based on ERA5. Spatial distributions of linear trends (**a**, **b**, and **c**) and time series (**d**, **e**, and **f**) of annual mean precipitation rate (Pr, **a** and **d**, unit: mm day^{-1}), surface air temperature (TS, **b** and **e**, unit: °C) and relative humidity (RH, **c** and **f**, unit: %) in Australia during 2010–2019 from ERA5 reanalysis. The shaded areas indicate trends are statistically significant at

804   the 90% confidence level. Regional averages over Australia are noted at the bottom-left corner of

805   panels a, b, and c. The p values and slopes of linear trends are noted in panels d, e, and f.

806

807

808   ~~Figure 3.~~

809
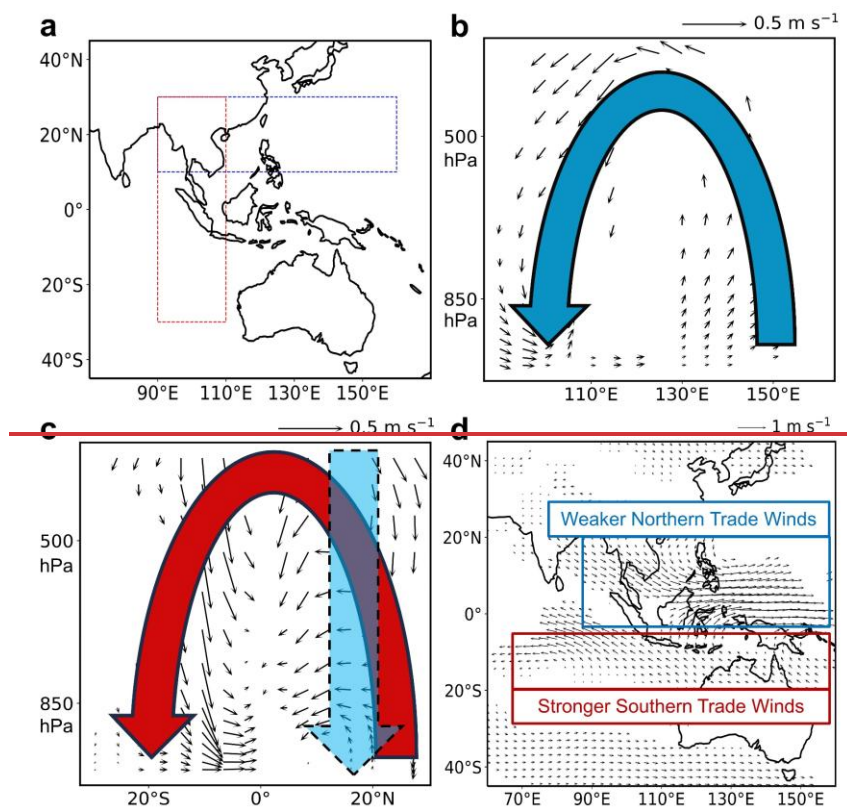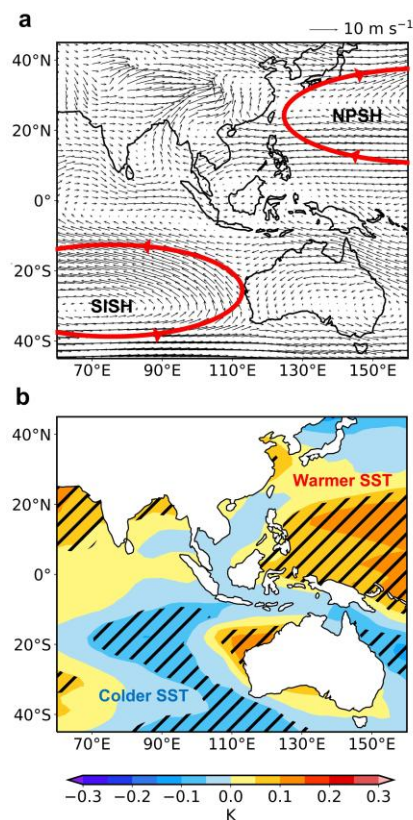
810 **Figure 4. Climatological mean wind fields at 850 hPa and Simulated sea surface temperature**

811 **changes due to aerosol changes in China between 2013 and 2019. a**, Climatological mean wind

812 fields (unit: m s^{-1}, vectors) at 850 hPa from the BASE experiment. NPSH and SISH shown in red

813 circles represents North Pacific Subtropical High and Southern Indian ocean Subtropical High,

814 respectively. **b**, Spatial distributions of simulated differences in annual mean sea surface

815 temperature (SST, unit: mm day^{-1}) in Australia between BASE and CHN (CHN minus BASE).

816 The shaded areas indicate results are statistically significant at the 90% confidence level.

817

818
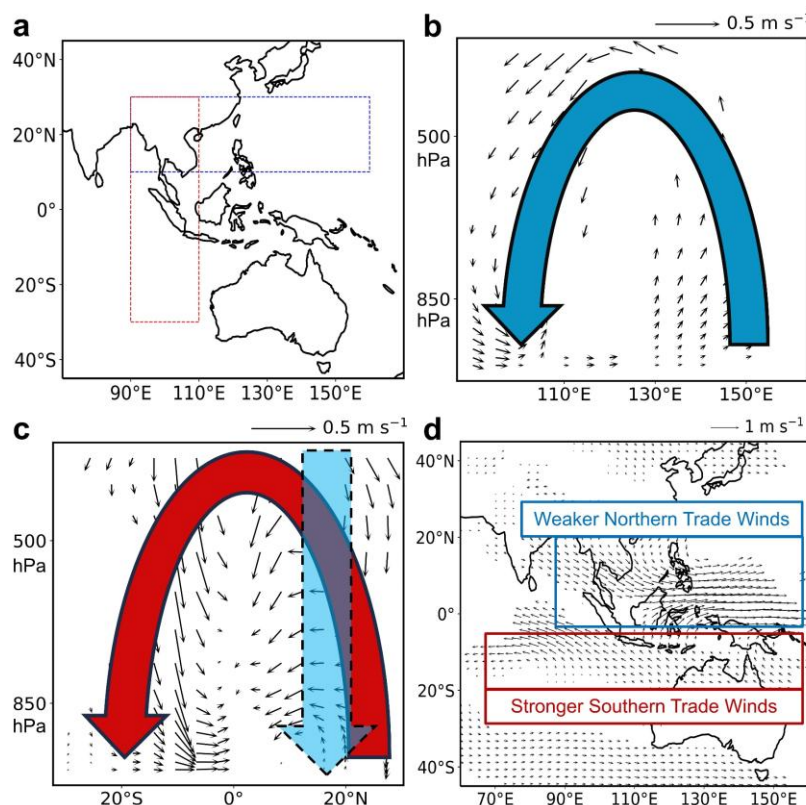
Figure 5. Simulated changes in vertical circulations and 850 hPa wind fields in Asia-Pacific regions due to aerosol changes in China between 2013 and 2019. Panel **b** and **c** shows pressure–longitude and pressure–latitude cross-section of responses in annual mean atmospheric circulations (unit: m s^{-1}, vectors), respectively, over the areas marked with the blue and red box in panel **a**. Panel **d** shows annual mean changes in wind fields (unit: m s^{-1}, vectors) at 850 hPa in Asia-Pacific regions. Only atmospheric circulations and winds statistically significant at the 90% confidence level are shown.

826

827

828   ~~Figure 4.~~
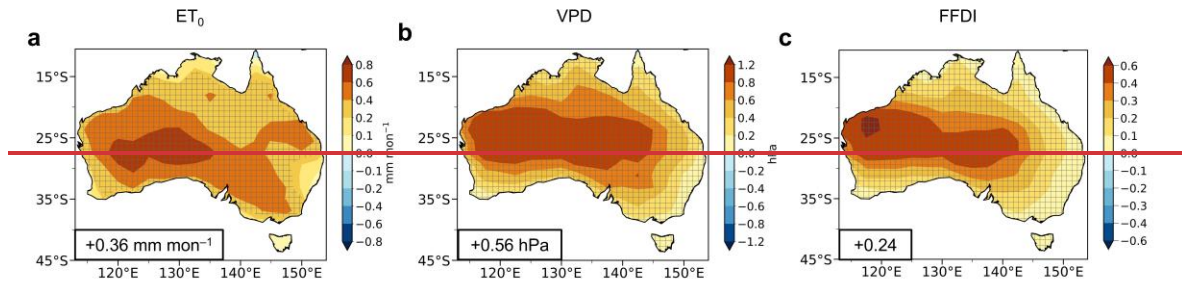
Figure 6. Schematic of the response in large-scale 3D circulations in the Asian-Pacific region to aerosol reductions in China. The top panel shows climatology mean condition, and the bottom panel shows anomalies resulting from aerosol reductions in China.
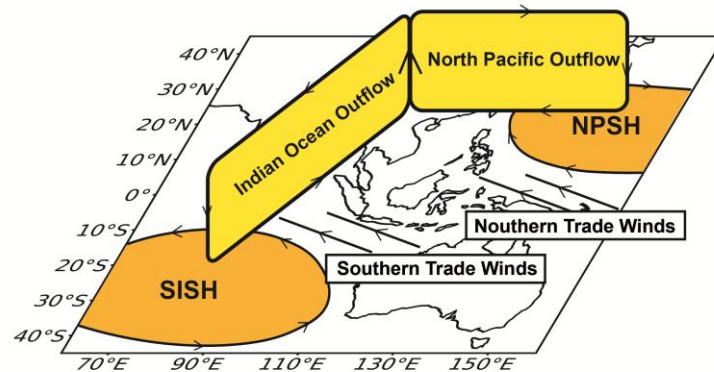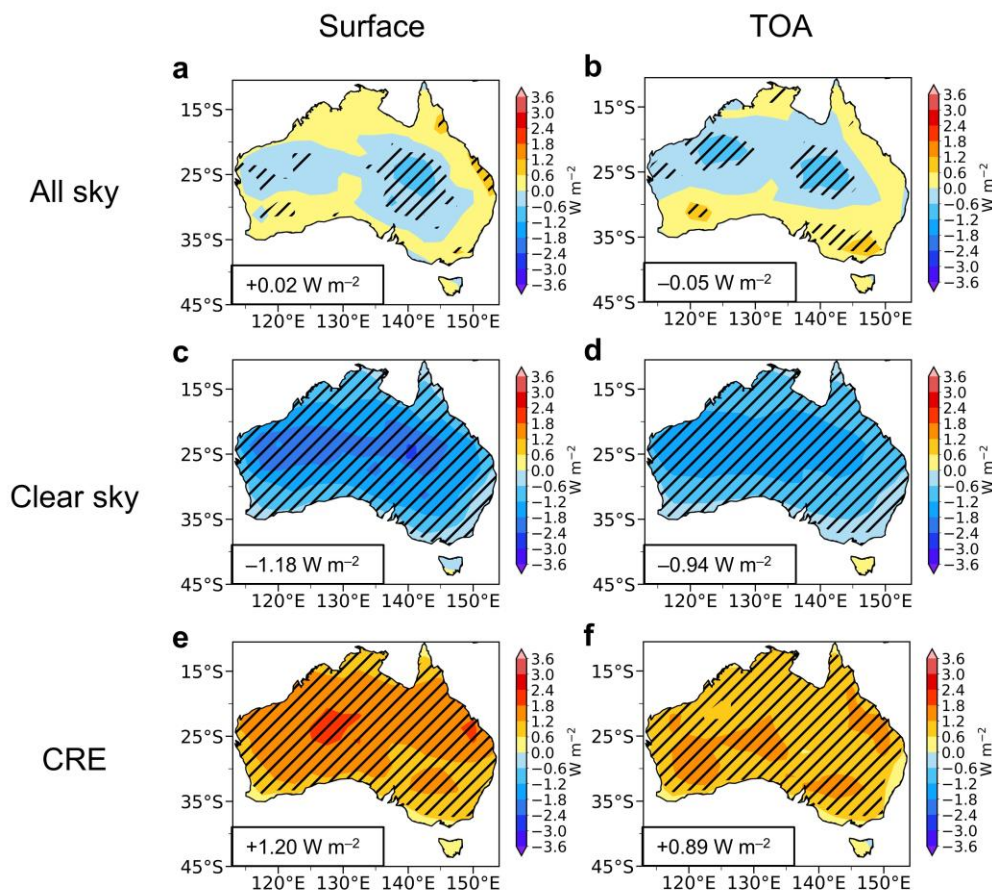
Figure 7. Simulated changes in surface and Top of the Atmosphere (TOA) net total radiative flux under all sky conditions, under clear sky conditions, and from cloud radiative effects in Australia due to aerosol changes in China between 2013 and 2019. Spatial distributions of simulated differences in annual mean surface (**a**, **c**, and **e**) and Top of the Atmosphere (TOA, **b**, **d**, and **f**) net total radiative flux (unit: W m^{-2}) under all sky conditions (**a** and **b**), under clear sky conditions (**c** and **d**), and from cloud radiative effects (CRE, **e** and **f**) in Australia between BASE and CHN (CHN minus BASE). Cloud radiative effects refer to differences under all sky and clear sky conditions (All sky minus Clear sky). The shaded areas indicate results are statistically significant at the 90% confidence level. Regional averages of the responses over Australia are noted at the bottom-left corner of each panel.
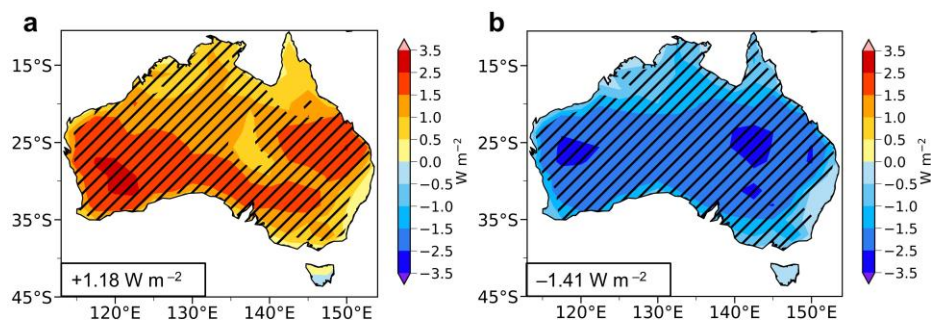
Figure 8. Simulated changes in surface upward sensible and latent heat flux in Australia due to aerosol changes in China between 2013 and 2019. Spatial distributions of simulated differences in annual mean surface upward sensible (**a**) and latent (**b**) heat flux (unit: W m^{-2}) in Australia between BASE and CHN (CHN minus BASE). The shaded areas indicate results are statistically significant at the 90% confidence level. Regional averages over Australia are noted at the bottom-left corner of each panel.
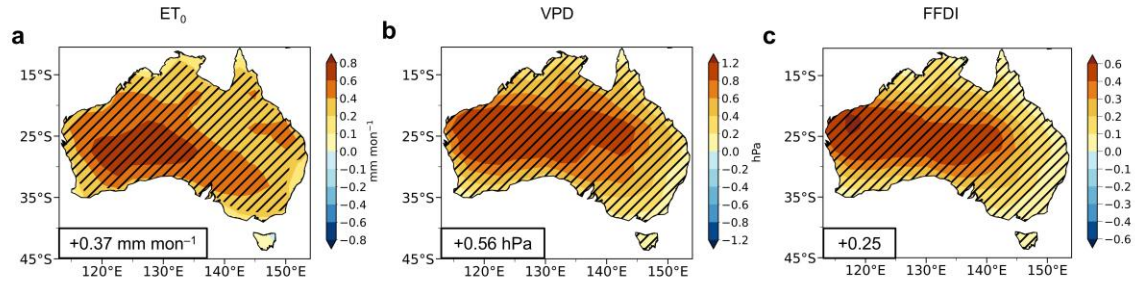
Figure 9. **Simulated changes in reference potential evapotranspiration, vapor pressure deficit, and McArthur forest fire danger index during fire seasons in Australia due to aerosol changes in China between 2013 and 2019.** Spatial distributions of simulated changes in reference potential evapotranspiration (ET$_0$, **a**, unit: mm mon^{-1}), vapor pressure deficit (VPD, **b**, unit: hPa), and McArthur forest fire danger index (FFDI, **c**, unitless) during fire seasons (austral spring and summer, from September to the February of the next year) in Australia between BASE and CHN (CHN minus BASE). The shaded areas indicate results are statistically significant at the 90% confidence level. Regional averages over Australia are noted at the bottom-left corner of each panel.